Highlight Review

Regulation of Interparticle Interaction of Metallic Nanoparticles Dispersible in Water: Dispersion, Controlled Assembly, and Formation of Particle Crystals

Keisaku Kimura

(Received April 2, 2009; CL-098005)

Abstract

Regulation of the lyophilicity and lyophobicity of a particle is very important for controlling interparticle interactions in solution. Through these interactions, we can precisely tune the formation of regular nanoparticle arrays and superlattices to create new materials. We demonstrate methods of controlling interparticle interactions that are effective for the formation of high-quality nanoparticle crystals. Unexpected electronic properties in high-quality superlattices were observed.

1. Introduction

Nanometer-scale materials are fascinating objects having a minimum unit of functionality, whose properties are different from atoms, molecules, and bulk materials. Nevertheless, they can be regarded as a bud for bulk diversity. In general, these materials are not thermodynamically stable, even if kinetically stable for hundreds of years like Faraday's gold sols. A high potential energy barrier among the isolated particles prohibits further coagulation of the sols. Since such sols are in a quasi-stable state, they must be kept at dilute concentrations and are not redispersible once dried when prepared by using techniques of traditional colloid chemistry. The surface state of this kind of classical sol is not fully understood because of a lack of analytical data from a molecular level. Recent developments in synthetic techniques using thiolate, phosphine, or amine derivatives to modify the surface of metallic particles have opened a new era for nanoscience in the materials world.[1–10] We can produce massive quantities of metallic sols of nanometer size in a condensed phase, which can be treated as a building block for functional architectures. The methods of synthesizing metallic nanoparticles have advanced due to the techniques of multiphase transport during the growth process. One such technique is phase transfer using the Brust methodology,[1] and another is phase separation by using thiol with a carboxylate moiety.[11,12] By virtue of the massive production of nanopowder, which is suitable for long-term storage, various applications have been realized such as the formation of supramolecular structures,[13–24] nanobased composite crystals,[25] and markers for biological pigments and sensors.[26,27]

A striking feature of the carboxylate-modified gold nanoparticles is that they are easily dispersible in water: a property that has not been achieved using other kinds of thiolate. A metallic nanoparticle itself can be regarded as a microelectrode.[28] Hence, it is very important to produce nanoparticles with a well-defined surface in order to understand the interaction of ions with an electrode surface at a molecular level. In order to construct a macroscopic entity from a nanosized material, it is essential to regulate the interparticle interactions between nanoparticles through the design of the surface ligands of the particles. In this article, we describe a method of controlling the interparticle interactions between metallic nanoparticles through the modification and design of the surface and tuning solution parameters under ambient conditions.

2. Nanometer-size Control

The synthesis of colloidal gold has been studied intensively for a long time.[29] A method developed by Brust et al.[1] to generate long-chain alkanethiolate-stabilized gold nanoparticles attracted considerable attention due to the superb stability of the particles; they are easily dispersible in organic solvent and can be reisolated as pure powders. Following this finding, much work has been devoted to modifying properties such as the reactivity and solubility of the nanoparticles by changing the molecular structures of the thiolates on the particle surface.[2–10] The method devised by Brust is based on phase transfer of chloroaurate from an aqueous solution to an organic solvent such as toluene, ether, or chloroform with the help of alkane thiolate. Gold sols were produced from chloroaurate by reduction with borohydride. This is effective for oil dispersion with a high concentration yield. The synthesis of oil-dispersed metallic nanoparticles is well established and does not need to be described here.

Another route to size control using thiolate is the phase-separation method developed in our laboratory[11,12] using a carboxylate or its derivatives as a residue (Scheme 1, MSA = mercaptosuccinic acid; MPG = *N*-(2-mercaptopropionylglycine; GTR = glutathione reduced form; NAG = *N*-acetylglutathione reduced form). Since the gold particles prepared by this method can be precipitated with poor solvent and redispersed in water without aggregation, we can easily narrow the size distribution with size-selective precipitation techniques[8,9] or stepwise size-selective extraction.[30] This makes them extremely attractive com-

Prof. Keisaku Kimura
Department of Material Science, Graduate School of Material Science, University of Hyogo, 3-2-1 Koto, Kamigori-cho, Ako-gun, Hyogo 678-1297
E-mail: kimura@sci.u-hyogo.ac.jp

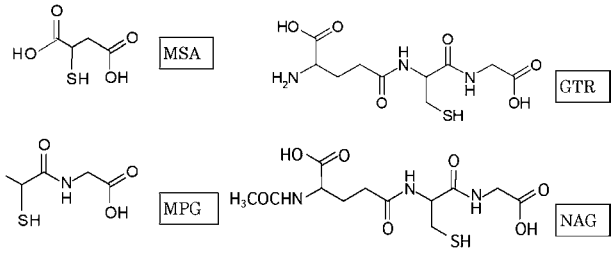

Scheme 1.

pared to other aqueous gold colloids, which often suffer the problem of easy aggregation and cannot be prepared in concentrated solutions.[29] In addition, the size of carboxylate-modified particles can be easily tuned by changing the mixing ratio of thiol to tetrachloroaurate tetrahydrate within a range from 0.5 to 2.5, which yields sizes between 1.2 and 3.4 nm. It is possible to achieve sizes smaller than 1 nm,[31,32] making these an excellent candidate as markers in cell-biological electron microscopy studies. The recovery rate or extraction rate of nanoparticles is also tuned by the composition ratio of the mixture of water to methanol (typically one to three (v/v)).

3. Surface Modification

Regulation of interparticle interactions is achieved in a tailored manner by the selection of suitable organic ligands. Through the selection of a particular thiolate functional group, the hydrophilicity, hydrophobicity, charged state, solubility, and redispersibility in a given solvent can be designed at a molecular level.

3.1 Reversible Dispersion from Powders

A remarkable characteristic of the self-assembled monolayer (SAM)-protected metallic nanoparticles is the redispersibility of dried sols. This is because the sols are protected with stable organic ligands that determine the stability of the sols against solvent. This feature is in stark contrast to a traditional sol. One such examples is the case of Au–MSA in which nanoparticles were dried under vacuum and then dispersed again, and this process was repeated again. We observed no change in the spectroscopic characteristics. Whereas in the case that gold nanoparticles were prepared by citric acid reduction and then surface species were replaced by MSA, noticeable coagulation occurred once the material was powdered. When we conducted the same experiment without substitution, irreversible coagulation took place and we could not observe the absorption spectrum of the sol any more.

3.2 Phase Transfer by Esterification of Surface Carboxylic Acid

Starting with particles having ligands such as MSA, we can modify the carboxylic acid moiety to contain an alkyl chain through an ester link with the use of a long-chain alcohol. Thus, the water dispersible nanopowder may change to an organo-dispersible powder. We will show one such procedure.[33] One point of caution is the stability of the metal–thiolate bond during the esterification reaction. Reduction of silver nitrate by sodium borohydride in the presence of MSA gives immediate production of silver nanoparticles modified with MSA. The typical size was

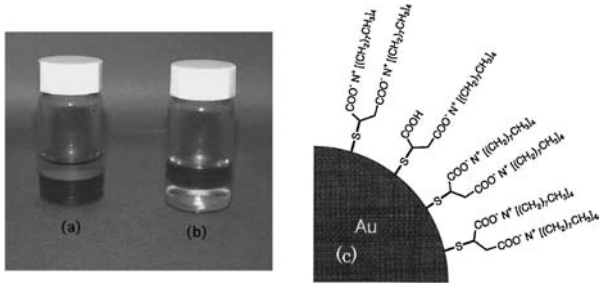

Figure 1. Photos of Ag dispersions: (a) before and (b) after esterification. Upper layer, *n*-butanol: lower layer, water for both bottles. (c) Schematic surface structure of transferred gold nanoparticles by stoichiometric ion-pair formation.

around 4 nm. *n*-Butanol was used as an esterification agent, and sulfuric acid was used as a catalyst. Almost no change was observed before and after the reaction by either visible absorption spectroscopy of the dispersion or transmission electron microscopic (TEM) observation of the particles formed. This affirms the stability of the thiolate linkage to silver. Photographs of the two dispersions are shown in Figures 1a with and 1b without esterification with butanol. These photographs clearly show the effects of the chemical modification. Elemental analysis by energy-dispersive X-ray spectroscopy (EDX) shows that 98% of MSA converted to MSA–butylacetate, which is comparable to finding no size change during the reaction. The same esterification reaction on the Au–MSA nanoparticles produced the same result. These facts indicate that metallic nanoparticles with well-characterized surfaces behave as if they were a common molecular compound.

3.3 Stoichiometric Ion-pair Formation

Unlike the esterification reaction, ion-pair formation based on electrostatic interaction between cationic tetraoctylammonium (TOA) in bulk solution and anionic carboxylate groups bound to the surface of the particles cause the phase transfer of water-dispersible gold nanoparticles into an organic phase. Thus, it is possible to extract nanoparticles successively from water to organic solvent by spontaneous formation of ion-pairs at the surface or the nanoparticles can migrate from the water phase to the organic phase.[30,34] EDX analysis revealed that 95% of the carboxylate anions of Au–MSA were stoichiometrically bound to TOA cations. This suggests the quantitative formation of SAM film on the nanoparticles. Thus, it is easy to control the surface functionality, reactivity, and dispersibility of nanoparticles by modifying the ion-pair reagents through this methodology. The surface structure estimated from elemental analysis is schematically illustrated in Figure 1c.[34] An electrostatic self-assembly strategy, that is, ion-pair formation, to make hybrid nanoparticles was attempted using amino-covered CdS and carboxylate-covered gold nanoparticles.[35] Efficient hybrid formation was observed.

3.4 Langmuir Adsorption Isotherm between Nanoparticles and Surfactants

Ion-pair formation between carboxylate anions on particle surfaces and TOA cations enables reversible control of the surface characteristics from hydrophilic to hydrophobic or vice versa. This reversibility is easily observed through the measure-

Published on the web (Advance View) June 27, 2009; doi:10.1246/cl.2009.754

ment of the adsorption isotherm. Typically in the gas phase, reversible adsorption/desorption processes are described by the Langmuir adsorption isotherm in the case of chemisorption as represented by the equation,

$$\frac{1}{\theta} = 1 + \frac{1}{KP} \text{ or } \frac{P}{x} = \frac{1}{Kb} + \frac{P}{b} \quad (1)$$

where θ is the coverage defined as the decimal fraction of adsorbed gas molecules x in relation to the saturation adsorption b, K is the equilibrium constant of the adsorption/desorption process, and P is pressure. In nanoparticle systems, TOA is the adsorbate and P is replaced by c, the concentration of TOA. We verified this equation by observing 2.7-nm Au–GTR nanoparticles as a function of TOA concentration and show the variation of the optical spectra in Figure 2a.[36] The absorption spectra of Au–GTR nanoparticles in the toluene layer are plotted at different TOA concentrations: a) 4×10^{-6} M, b) 1×10^{-5} M, c) 2.2×10^{-5} M, d) 3.2×10^{-5} M, e) 6.4×10^{-5} M, and f) 1.2×10^{-4} M. Figure 2b shows the change of the absorbance at 514 nm (the position of the surface plasmon resonance absorption peak) in toluene (○) and water (●) layers, respectively. The open circles represent the portion of gold particles transferred into the toluene layer, which is proportional to the number of adsorbed TOA assuming complete coverage. The concentration of TOA at maximum coverage well matched with the total transference of gold particles as arrow marked in Figure 2b, showing a point of full monolayer adsorption. This follows the relation of the equation, thus justifying our assumption. From the slope and intercept of the c/x–c plot as shown in Figure 2c, we determined the saturation adsorption and K. Knowing the amount of particles in solution, the surface area and the given parameters, we calculated the number of –COO– and adsorbed TOA cations. These two values roughly coincide with each other indicating that stoichiometric ion-pair formation and a reversible adsorption process occur.

4. Controlled Assembly at an Interface

4.1 Strain-free Crystal Growth at an Air/Water Interface

Liquids have the highest symmetry and as a result, there is no definite lattice vector. In other words, there is no lattice mismatching if crystal growth takes place on a liquid surface. Therefore, crystal growth on a liquid surface instead of a solid substrate is ideal for strain- or stress-free processes. The selection of thiolate is crucial for controlling this process. In particular, the balance of hydrophilicity (charged state in solution) and hydrophobicity (charge neutrality in air) of the ligand is important. This is the basic concept of our superlattice formation. We present two examples relating to this subject.

Figure 3 shows TEM images of the different stages of the growth process of Au–MSA nanoparticles forming particle crystals (superlattice) in a monolayer, double layer, and multilayer formation at an air/water interface following the addition of HCl.[37] A layer-by-layer growth process is apparent. Initially, the domain size is less than 30 nm with a size distribution of 14%. Later, the distribution narrows to 4%. The size of the particles, 3.5 nm, is almost unchanged during the process. This self-correcting process is highlighted in the case of Ag nanoparticle crystal growth.[38,39] Even starting from particles with 30% polydispersity, we obtain particle crystals having a narrower size distribution of 13% using vapor diffusion. In Figure 4, this process is shown schematically. Typical conditions for equilibrium growth are 4.0 mg of gold nanoparticle powder in 2.0 mL of 0.2–0.3 M HCl in a closed glass vial that prevents the solvent from evaporating. Under these conditions, a lattice appears in 5 days.[23] As shown in Figure 4b, HCl is added to weaken the repulsion among the nanoparticles in the solution, but the repulsion is primarily lowered at the interface (Figure 4a) due to the hydrophobicity of air. Hydrogen-bonding interactions among particles may reinforce the ubiquitous van der Waals interactions that are the main origin of attractive force. Thus, the interparticle interactions can be controlled by external parameters such as pH and the ionic strength of the solution. It should be noted that the self-correcting process requires long growth times to yield a macroscopic crystal. In fact, crystal growth of several micrometers requires several days for Au–MSA and several months for Au–NAG.

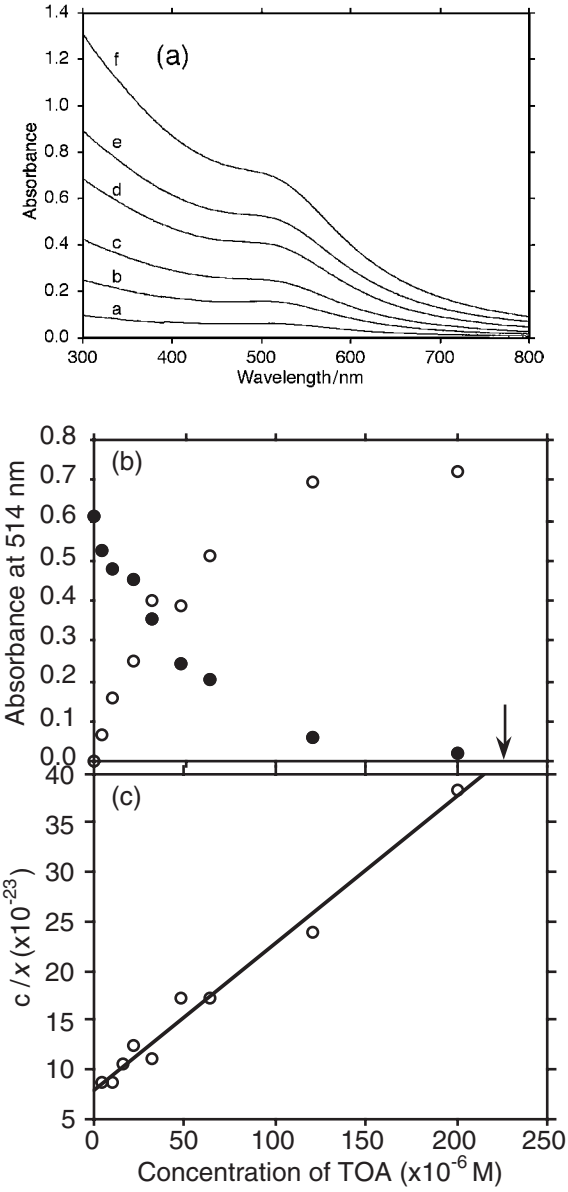

Figure 2. Adsorption isotherm of Au nanoparticle in water.

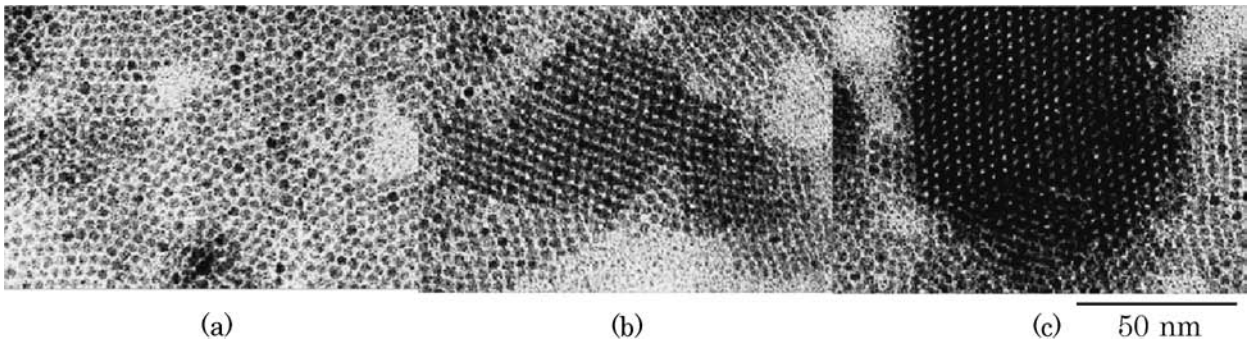

Figure 3. Layer-by-layer growth process. (a) Monolayer, (b) double layer, and (c) multilayer.

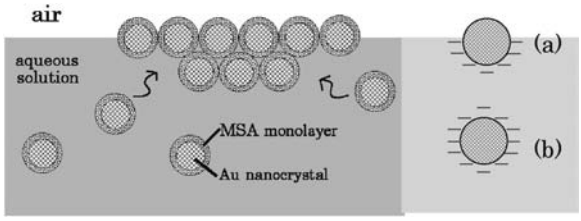

Figure 4. Superlattice formation at the interface. (a) Upper hemisphere is neutral, (b) whole surface is negatively charged inducing strong repulsion.

4.2 Morphological Control by Gas and Temperature

We also investigated the effects of the surrounding gas on the self-assembly process since self-assembly occurs at the gas/suspension interfaces as illustrated in Figure 4. In addition to the Au–MSA dispersions in aqueous HCl solution, the remaining volume in the vials was filled with air, nitrogen, oxygen, or a mixture of air and saturated organic vapor at room temperature. The total pressure in the sealed vials was 1 atm. After 4 days at room temperature, various assemblies form that are dependent on the experimental conditions.[40] The assemblies formed on the suspension surfaces were examined by scanning electron microscopy (SEM), X-ray diffraction (XRD), and EDX. It was found that the morphology of the self-assembled gold nanoparticles is greatly affected by the components of the gas species. SEM photos are shown in Figure 5.[40] In air, oxygen, or nitrogen, high-quality particle crystals possessing hexagonal, triangular, or diamond-like shapes grow at the gas/suspension interfaces (Figure 5a). The thickness of the superlattices ranges from 0.2 to 5 μm. When organic vapor was introduced into the gas phase, no particle crystal with sharp facets was observed at the gas/suspension interface. Spherical aggregates made of gold nanoparticles with diameters of several micrometers formed when the gas phase contained nonpolar organic molecules such as pentane, hexane, octane, or cyclohexane (Figure 5b). On the other hand, irregularly shaped aggregates of gold nanoparticles formed (Figure 5c) when the gas phase contained polar organic vapors such as acetonitrile or chloroform. Therefore, an assembly of gold nanoparticles with controllable dimension at the gas/suspension interfaces can easily be achieved by controlling the components of the environmental gas phase. Structural information of the obtained aggregates was measured by XRD in the small angle region (SAXRD). The SAXRD patterns confirmed that the MSA-coated gold nano-

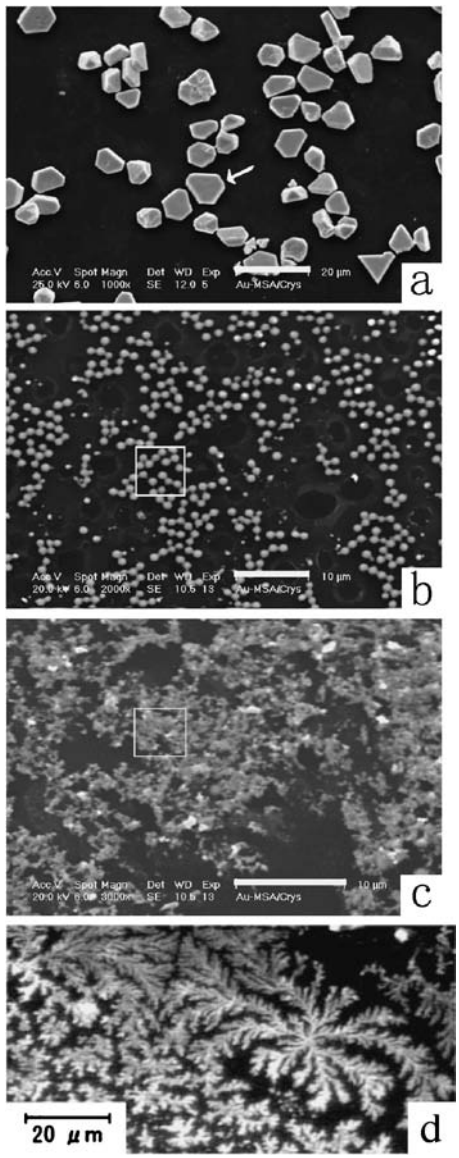

Figure 5. Morphology regulation by gas (a)–(c) and temperature (d). Scale bar; 20 μm (a), (d) and 10 μm (b), (c).

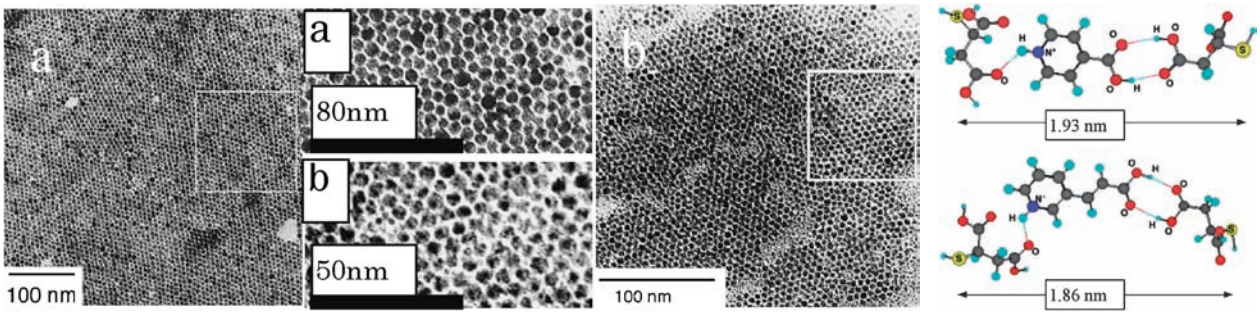

Figure 6. (a) Au–PyC–SL and (b) Au–PyA–SL. Panels a and b are for TEM micrographs. Right panels are optimized molecular geometry.

particles in the spherical assemblies (Figure 5b) and in the irregular shaped aggregates (Figure 5c) are randomly arranged. However their contents did not change from component nanoparticles used as EDX analyses evidenced (rectangular area in Figures 5b and 5c.)

The temperature of the suspension strongly affects the assembly process of the gold nanoparticles.[41] High-quality lattice arrangements were obtained below 30 °C and an HCl concentration between 0.2 and 0.3 M. At temperatures higher than 30 °C, the nanoparticles form dendritic patterns (Figure 5d), which may result from the diffusion-limited aggregation (DLA) of particles on the suspension surface.[42] This increasing attractive interaction with increasing temperature is characteristic of the interaction between hydrophobic surfaces in water.[43,44] Therefore, the accumulation of nanoparticles at the interface appears to be due to the hydrophobic effect,[45] which results from the nanoparticle surfaces being converted from hydrophilic to hydrophobic. Note that the ionization of the MSA surface layers is significantly suppressed by the addition of HCl. This also explains why nanoparticles are assembled at the air/aqueous solution surface considering that air itself is hydrophobic in nature.[45]

4.3 *Insertion of Hydrogen-bonding Mediators into the Particle Array*

The system we have discussed consists of hydrophilic nanoparticles with strong hydrogen-bonding and/or electrostatic interactions. In particular, hydrogen-bonding interactions are known to be attractive and directionally specific and offer a controllable pathway for structural manipulation of assembly[46–48] as is observed in the highly regular structures of polypeptides consisting of amino acids that are the building blocks of all living species. Therefore, we inserted a hydrogen-bonding mediator molecule into the nanoparticle network to control the interparticle interactions. Two mediator molecules (4-pyridinecarboxylic acid (PyC) and *trans*-3-(3-pyridyl)acrylic acid (PyA)) were found to effectively modify the Au–MSA superlattice.[49] Figure 6 shows the TEM micrographs of superlattices prepared in the presence of PyC and PyA. The boxed area is magnified and displayed in the center of Figure 6. Calculations of the optimized stable geometry of a "triad" show that one hydrogen-bonding mediator is incorporated between two MSA molecules through hydrogen bonding. These results are shown in Figure 6. The sulfur–sulfur distances (shown as arrows in Figure 6) of MSA–mediator–MSA are 1.93 and 1.86 nm for Au–PyC–SL and Au–PyA–SL, respectively. These values are consistent with the value obtained by subtracting the core size from the lattice constant from TEM measurements. Thus, we can design the particle spacing, that is, the lattice constant of the superlattice, by insertion of hydrogen-bonding mediator molecules, which allows the design of the electronic state of the superlattice.

5. High-quality Superlattice Formation at the Interface

5.1 *Structure and Morphology of Particle Crystals*

The particle crystals grown at the air/water interface are shown in Figure 5a for Au–MSA. SAXRD of the gold particle crystals clearly shows nanometer-scale periodicity. It was also noted that only a selected number of facets appear in the diffraction, suggesting that all superlattices align along a specific axis on the substrate. Some of the close-up photos of the particle crystals made of Au–NAG are shown in Figure 7. The majority of the morphologies of the superlattices have threefold symmetry such as triangular or hexagonal plates, triangular prisms or tetrahedra (Figure 7 left). However, it is noteworthy that there are several superlattices with fivefold symmetry such as pentagonal rods, decahedra, and Marks decahedra (Figure 7 center) and icosahedra (Figure 7 right). This is the first observation of *fivefold symmetry* in a nanoparticle superlattice.[50] Nanometer resolution images by FESEM revealed that the majority of the triangular faces are the close-packed {111}-like plane, whereas the truncated face is a tetragonal {112}-like plane. For a regular decahedron, there is a large surface/volume ratio, which can be lowered by truncating the edges around the common base. Marks decahedra are preferentially obtained by introducing reentrances that separate the {100}-like facets as seen in Figure 7 center.[51] Note that the size of the superlattices with a fivefold axis is around 5 μm, while the sizes of icosahedra or decahedra consisting of atoms are 30 or 300 nm, respectively. This suggests a large relaxation of internal strain in particle assemblies.

5.2 *Optical Properties of Quality Particle Crystals*

In the following section, we examine the effects of ligands on the electronic state of superlattices.[52] Three kinds of nanoparticle superlattices were prepared according to standard procedures. The SEM images (Figure 8, Left) show diverse shapes such as triangular (labeled T) or hexagonal (H) plates, as well as diamond-like (D) or pyramidal (P) shapes. For all the ligands examined, superlattices appeared at the air/water interface as described in Section **4**. High-resolution TEM (HRTEM) clearly

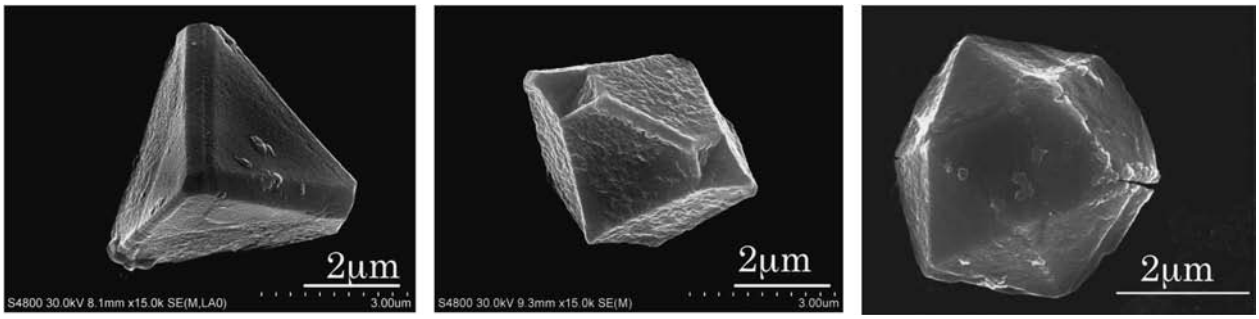

Figure 7. Examples of 3D superlattice of Au–NAG nanoparticles.

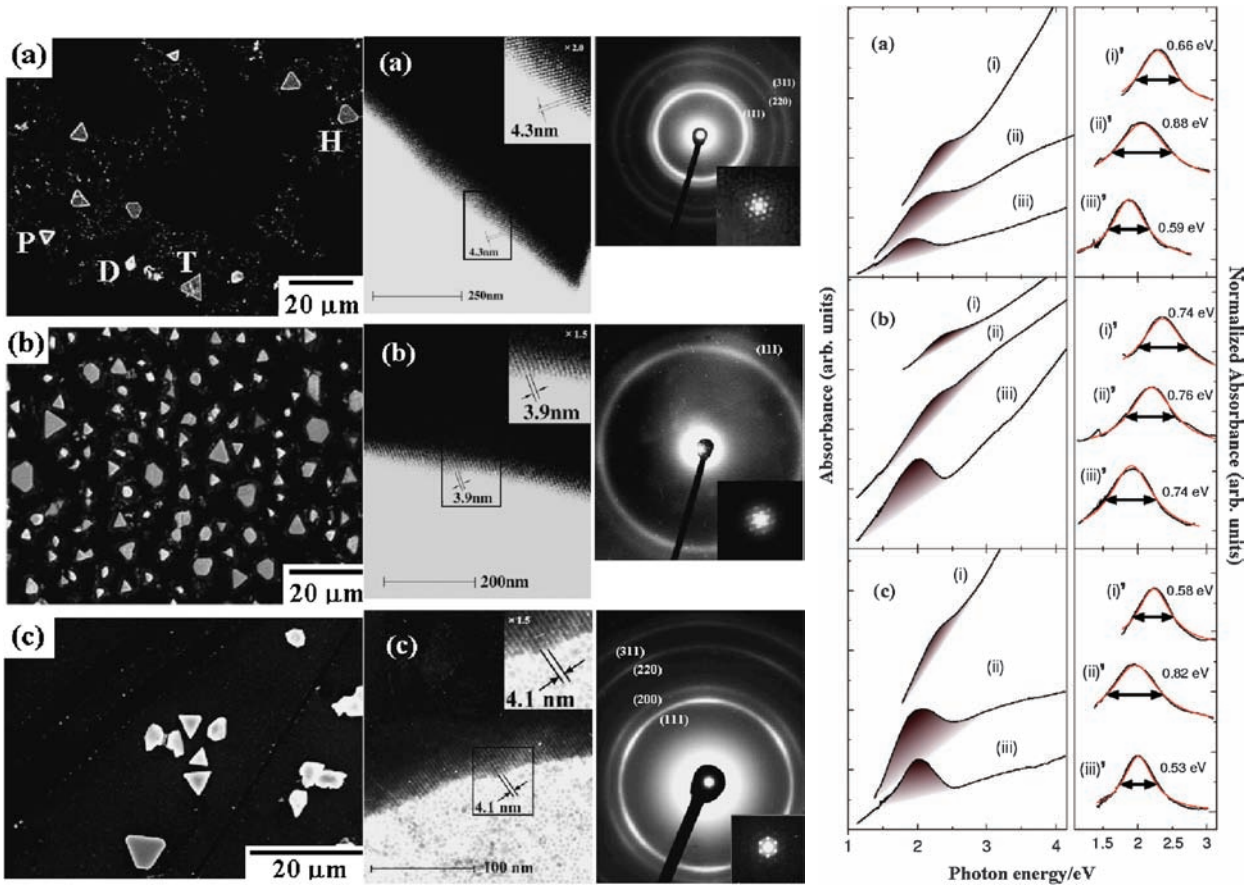

Figure 8. Left panel is for SEM, HRTEM, and TED of (a) Au–MSA, (b) Au–MPG, and (c) Au–NAG superlattices. Inset in HRTEM is a magnified image of boxed area. Inset in TED is low-angle TED. Right panel is for optical absorption spectra of the same particles. Right spectra are those after subtraction of background. Red lines are derived from the imaginary part of the dielectric function used.

shows that these superlattices consist of nanoparticles whose size is on the order of nanometers. As seen in the low-angle and wide-angle XRD (not shown) and transmission electron diffraction (TED) patterns, the assemblies exhibit double periodicity (and are thus called superlattices) originating from atomic alignment on the angstrom scale and the alignment of nanoparticles on the nanometer scale as shown by the inset in the TED images. The former periodicity corresponds to the lattice spacing of bulk Au, and the rings in the TED were successfully indexed based on the lattice constants of bulk gold. We noticed that there was a fifth Bragg diffraction in the inset of TED of Au–MSA, which indicates high-quality superlattice formation. It should also be noted that arc patterns appeared in the wide-angle TED (WATED) region in the case of the Au–NAG superlattice. This reflects the fact that there is orientational ordering or preferential orientation in addition to translational ordering of nanoparticles in the superlattice. That is to say, *gold atoms* more or less align orderly over the superlattice space. We can deduce structural information on the superlattice such as rotational misfit among lattice planes with precise examination of this pattern.[53]

Figure 8 also shows the optical absorption spectra of three kinds of aggregation states: (i) dispersed in water, (ii) random aggregates, and (iii) superlattice assemblies with the three modi-

fier thiolates. All of the dispersed nanoparticles exhibited small peaks at 2.2–2.4 eV, which correspond to the surface plasmon resonance (SPR) energy of gold. As the nanoparticles densely assemble, the peaks red-shift and intensify. Such peak shifts can be explained using the classical theory of electronic polarizability. Assuming that the nanoparticles are simple harmonic oscillators, the dielectric function of the superlattices composed of these artificial atoms is given by a phenomenological equation with two fitting parameters, plasmon frequency and the damping factor, Γ. The best fit gave the red lines in Figure 8. It is notable that Γ increases when the nanoparticles randomly assemble but decreases after forming a superlattice.[54] Taking account of the fact that the Γ values of the superlattices become smaller than those of the dispersed nanoparticles, extended dipole–dipole interaction or a large electric dipole might form in the superlattices. This observation resembles the coherent migration of excitons in CuCl crystals or J-band formation in molecular crystals of cyanine dye. Thus, the inherently broad absorption of SPR tends to sharpen the absorption band. We emphasize that these properties are common to all three samples regardless of the differences in the ligand molecules. This is a characteristic of high-quality superlattices.

6. Summary and Future Prospects

The modification of the lyophilicity and lyophobicity of metallic nanoparticles is demonstrated by two methods, an esterification reaction of a carboxylic acid of a surface thiolate and a stoichiometric ion-pair formation between a carboxylate anion and a cationic surfactant. Thanks to this modification, metallic nanoparticles can transfer from the aqueous phase to the organic phase or vice versa. It was also demonstrated that interparticle interaction can be tuned by external parameters such as temperature or atmosphere via the use of nanoparticles modified with molecular-level precision. Thus, we can obtain a quality particle crystal through an appropriate combination of parameters that sharpen the surface plasmon resonance absorption band. In addition to these fundamental techniques, by expanding our research to mixtures of different types of nanoparticles such as a ternary system, more complicated structures can possibly be assembled. This would lead to novel electronic structures and properties. The realization of self-assembled electronic devices is our ultimate goal.

This research was supported by Grants-in-Aid for Scientific Research [S: No. 16101003, B: No. 13440212] from the Japan Society for the Promotion of Science and Scientific Research in Priority Areas [Application of Molecular Spins: No. 15087210] from MEXT. The author is very grateful to the collaborators of his research group, whose names appear in the papers referenced in this article for their invaluable cooperation and input.

References and Notes

1 M. Brust, M. Walker, D. Bethell, D. J. Schiffrin, R. Whyman, *J. Chem. Soc., Chem. Commun.* **1994**, 801.
2 M. Brust, J. Fink, D. Bethell, D. J. Schiffrin, C. Kiely, *J. Chem. Soc., Chem. Commun.* **1995**, 1655.
3 S. R. Johnson, S. D. Evans, S. W. Mahon, A. Ulman, *Langmuir* **1997**, *13*, 51.
4 M. J. Hostetler, S. J. Green, J. J. Stokes, R. W. Murray, *J. Am. Chem. Soc.* **1996**, *118*, 4212.
5 R. S. Ingram, M. J. Hostetler, R. W. Murray, *J. Am. Chem. Soc.* **1997**, *119*, 9175.
6 P. A. Buining, B. M. Humbel, A. P. Philipse, A. J. Verkleij, *Langmuir* **1997**, *13*, 3921.
7 L. O. Brown, J. E. Hutchison, *J. Am. Chem. Soc.* **1997**, *119*, 12384.
8 C. B. Murray, D. J. Norris, M. G. Bawendi, *J. Am. Chem. Soc.* **1993**, *115*, 8706.
9 T. Vossmeyer, L. Katsikas, M. Giersig, I. G. Popovic, K. Diesner, A. Chemseddine, A. Eychmueller, H. Weller, *J. Phys. Chem.* **1994**, *98*, 7665.
10 X. M. Lin, C. M. Sorensen, K. J. Klabunde, *Chem. Mater.* **1999**, *11*, 198.
11 S. Chen, K. Kimura, *Langmuir* **1999**, *15*, 1075.
12 S. Chen, K. Kimura, *Chem. Lett.* **1999**, 1169.
13 C. B. Murray, C. R. Kagan, M. G. Bawendi, *Science* **1995**, *270*, 1335.
14 M. Brust, D. J. Schiffrin, D. Bethell, C. J. Kiely, *Adv. Mater.* **1995**, *7*, 795.
15 R. L. Whetten, J. T. Khoury, M. M. Alvarez, S. Murthy, I. Vezmar, Z. L. Wang, P. W. Stephens, C. L. Cleveland, W. D. Luedtke, U. Landman, *Adv. Mater.* **1996**, *8*, 428.
16 J. Fink, C. J. Kiely, D. Bethell, D. J. Schiffrin, *Chem. Mater.* **1998**, *10*, 922.
17 S. A. Harfenist, Z. L. Wang, R. L. Whetten, I. Vezmar, M. M. Alvarez, *Adv. Mater.* **1997**, *9*, 817.
18 A. Taleb, C. Petit, M. P. Pileni, *Chem. Mater.* **1997**, *9*, 950.
19 J. R. Heath, C. M. Knobler, D. V. Leff, *J. Phys. Chem. B* **1997**, *101*, 189.
20 A. Taleb, C. Petit, M. P. Pileni, *Chem. Mater.* **1997**, *9*, 950.
21 A. Taleb, C. Petit, M. P. Pileni, *J. Phys. Chem. B* **1998**, *102*, 2214.
22 M. P. Pileni, *J. Phys. Chem. B* **2001**, *105*, 3358.
23 K. Kimura, S. Sato, H. Yao, *Chem. Lett.* **2001**, 372.
24 S. Wang, S. Sato, K. Kimura, *Chem. Mater.* **2003**, *15*, 2445.
25 E. V. Shevchenko, D. V. Talapin, N. A. Kotov, S. O'Brien, C. B. Murray, *Nature* **2006**, *439*, 55.
26 M. A. El-Sayed, *Acc. Chem. Res.* **2001**, *34*, 257.
27 Articles in the Special Issue of Synthesis and Plasmonic Properties of Nanostructures: *MRS Bull.* **2005**, *30*, No. 5.
28 A. Henglein, *Chem. Rev.* **1989**, *89*, 1861.
29 *Colloidal Gold: Principles, Methods and Applications*, ed. by M. A. Hayat, Academic Press, San Diego, CA, **1989**, Vols. 1 and 2.
30 H. Yao, O. Momozawa, T. Hamatani, K. Kimura, *Chem. Mater.* **2001**, *13*, 4692.
31 Y. Negishi, Y. Takasugi, S. Sato, H. Yao, K. Kimura, T. Tsukuda, *J. Am. Chem. Soc.* **2004**, *126*, 6518.
32 Y. Negishi, K. Nobusada, T. Tsukuda, *J. Am. Chem. Soc.* **2005**, *127*, 5261.
33 J. Tominaga, S. Sato, H. Yao, K. Kimura, *Chem. Lett.* **2002**, 950.
34 H. Yao, O. Momozawa, T. Hamatani, K. Kimura, *Bull. Chem. Soc. Jpn.* **2000**, *73*, 2675.
35 S. Chen, K. Kimura, *Chem. Lett.* **1999**, 233.
36 S. Chen, H. Yao, K. Kimura, *Langmuir* **2001**, *17*, 733.
37 S. Sato, H. Yao, K. Kimura, *Physica E* **2003**, *17*, 521.
38 Y. Yang, S. Liu, K. Kimura, *Angew. Chem., Int. Ed.* **2006**, *45*, 5662.

39 Y. Yang, K. Kimura, *J. Phys. Chem. B* **2006**, *110*, 24442.
40 S. Wang, S. Sato, K. Kimura, *Chem. Lett.* **2003**, *32*, 520.
41 S. Sato, S. Wang, S. Kinugasa, H. Yao, K. Kimura, in *Physics, Chemistry and Application of Nanostructures*, ed. by V. E. Borisenko, S. V. Gaponenko, V. S. Gurin, World Scientific, **2003**, pp. 313–319.
42 T. Vicsek, *Fractal Growth Phenomena*, World Scientific, Singapore, **1989**.
43 P. M. Claesson, R. Kjellander, P. Stenius, H. K. Christenson, *J. Chem. Soc., Faraday Trans. 1* **1986**, *82*, 2735.
44 Z. Xu, R.-H. Yoon, *J. Colloid Interface Sci.* **1990**, *134*, 427.
45 J. N. Israelachvili, in *Intermolecular and Surface Forces*, 2nd. ed., Academic Press, **1992**, Secs. 6 and 11.
46 E. Hao, T. Lian, *Chem. Mater.* **2000**, *12*, 3392.
47 Y. Kim, R. C. Johnson, J. T. Hupp, *Nano Lett.* **2001**, *1*, 165.
48 L. Han, J. Luo, N. N. Kariuki, M. M. Maye, V. W. Jones, C. J. Zhong, *Chem. Mater.* **2003**, *15*, 29.
49 H. Yao, H. Kojima, S. Sato, K. Kimura, *Langmuir* **2004**, *20*, 10317.
50 H. Yao, T. Minami, A. Hori, M. Koma, K. Kimura, *J. Phys. Chem. B* **2006**, *110*, 14040.
51 L. D. Marks, *Philos. Mag. A* **1984**, *49*, 81.
52 T. Oonishi, S. Sato, H. Yao, K. Kimura, *J. Appl. Phys.* **2007**, *101*, 114314.
53 S. Sato, S. Wang, K. Kimura, *J. Phys. Chem. C* **2007**, *111*, 13367.
54 M. Quinten, U. Kreibig, *Surf. Sci.* **1986**, *172*, 557.